Journal of Molecular Graphics and Modelling 32 (2012) 1–8

Contents lists available at SciVerse ScienceDirect

Journal of Molecular Graphics and Modelling

journal homepage: www.elsevier.com/locate/JMGM

The structure–property relationship of chiral 1,1′-binaphthyl-based polyoxometalates: TDDFT studies on the static first hyperpolarizabilities and the ECD spectra

Jian-Ping Wang, Li-Kai Yan, Wei Guan, Shi-Zheng Wen, Zhong-Min Su*

Institute of Functional Material Chemistry, Faculty of Chemistry, Northeast Normal University, Changchun 130024, PR China

ARTICLE INFO

Article history:
Received 25 June 2011
Received in revised form
14 September 2011
Accepted 16 September 2011
Available online 22 September 2011

Keywords:
Binaphthol
Polyoxometalate
Enantiomer
Nonlinear optics
High-dimensional

ABSTRACT

In this paper, density functional theory is used to investigate the linear optical and nonlinear optical (NLO) properties of a series of Λ-type chiral compounds composed of two Lindqvist-type polyoxometalates (POMs) linked by 1,1′-binaphthyl derivatives through arylimido. It shows that compound **1** which has two POMs on 6-6′-sites of 1,1′-binaphthyl possesses large static first hyperpolarizability and the strongest two-dimensional NLO response among studied compounds. The organic substituents on 2-2′-sites of 1,1′-binaphthyl twofold control the NLO responses of studied compounds. They act as electron acceptors or donors therefore suppress or enhance the NLO responses of studied compounds, and they restrain the torsion angles between two naphthyl rings at certain degrees which are inversely proportional to the NLO responses. Compound **6** with remarkable NLO response is obtained as ferrocene substitutes on 2-2′-sites of 1,1′-binaphthyl. Additionally, the electronic circular dichroism (ECD) spectra of studied compounds are simulated with CAM-B3LYP and B3LYP hybrid functionals. The results agree well with the experimental ECD spectra. The charge-transfer transitions from organic fragment to POM are responsible for the ECD differences between molecular hybrids and their precursors. It is confirmed that these Λ-type chiral compounds are potentially high-dimensional NLO materials and the structure–property relationship of these compounds is presented.

1. Introduction

Polyoxometalates (POMs) are early transition-metal (usually W^{VI}, Mo^{VI}, and V^{V}) oxide with the extensive capability of attaching organic groups on the surface of the cluster [1]. If suitable organic ligands are available, they can be exploited to make chiral POM derivatives. These chiral derivatives have attracted much attention in scientific research fields due to their merits in asymmetric catalysis [2], molecular recognition [3], and marvelous structures [4]. Recently, many chiral POM derivatives have been synthesized and characterized by electronic circular dichroism (ECD) spectra [5–8]. In spite of the splendid studies in experiment, the quantum chemical studies of chiral POMs are few [9]. Moreover, chiral molecules have been exploited and modified to show nonlinear optical (NLO) responses [10]. It is prior that chiral molecules seldom pack into crystals in center space group due to their inherent noncentrosymmetry, which is necessary to generate electric-dipole-allowed second-order NLO response. In the cases of helical-shaped molecules, the magnetic-dipole and quadrupole contributions to NLO responses are significant compared with the electric-dipole contributions, therefore the NLO responses are further enhanced [11]. Another interesting character of chiral molecule in nonlinear optics is that the optical activity can be observed based on nonlinear process [12]. The NLO activity is more sensitive than linear optical activity. Thus techniques based on nonlinear optical activities are increasingly applied to detect the surface chirality [13] and the second-order structures of protein and DNA [14,15].

In 1996, the NLO response of POM was firstly observed by Niu et al. in noncentrosymmetric-space-group crystal of Keggin-type POMs and organic substrates, and the third-order susceptibilities were studied [16]. Traditionally, large NLO response molecules are those chromophores composed of electron donors and acceptors, which are linked through an intervening π-bridge [17]. POMs have been the subject of NLO studies [18–20]. The NLO responses of POMs were improved through directional design and synthesis [21–23]. The theoretical studies on NLO properties of POM-based compounds have been systematically carried out by our group using time-dependent density functional theory (TDDFT) methods [24,25]. The π-bridge lengths were optimized to improve the second-order NLO response [26], and different organic substituents

* Corresponding author. Tel.: +86 431 85099108; fax: +86 431 85684009.
E-mail addresses: yanlk924@nenu.edu.cn (L.-K. Yan), zmsu@nenu.edu.cn (Z.-M. Su).

1093-3263/$ – see front matter © 2011 Elsevier Inc. All rights reserved.
doi:10.1016/j.jmgm.2011.09.005

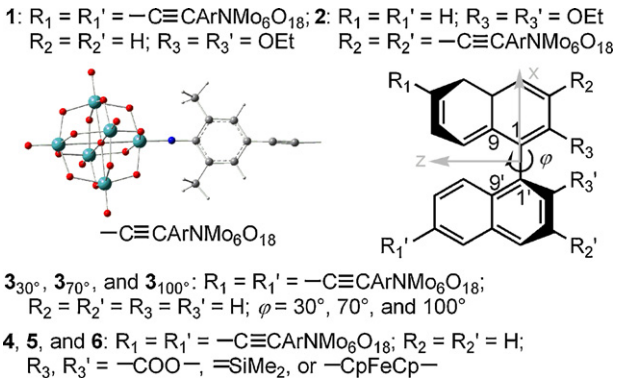

Fig. 1. The calculation models.

combined with the π-bridge were studied to give different electron transitions and NLO responses [20]. Recently, we investigated the NLO properties of Λ-type POM derivatives, which are based on the reversible metal-centered redox process. The results show that this kind of derivatives is promising candidates for two-dimensional-NLO (2D-NLO) materials [27].

1,1′-Binaphthyl has been widely used to generate novel chiral materials [28,29]. It can be used as a bridge to link two Lindqvist-type polyanions through π-bridge arylimido, therefore Λ-type compounds **1** and **2** are formed (Fig. 1) [30]. These chiral compounds are potentially multifunctional materials bearing NLO responses. On the basis of this structural regime, we design several analogs (compounds **4**, **5**, and **6** in Fig. 1) by introducing different electron acceptors and donors on 2,2′-sites of 1,1′-binaphthyl to investigate the influence of electron acceptor–donor substitutions on NLO responses. Moreover, the torsion angle between two naphthyl rings is fixed at different degrees (compounds $\mathbf{3}_{30^\circ}$, $\mathbf{3}_{70^\circ}$, and $\mathbf{3}_{100^\circ}$ in Fig. 1) to detect the influence of conjugation on NLO responses. In this work, the second-order NLO properties of Λ-type binaphthyl–hexamolybdate compounds are investigated by using TDDFT methods. The linear optical activities of compounds **1** and **2** and their precursors 1,1′-bi-6,6′-ethynyl-2,2′-binaphthol ($\mathbf{1}_{\text{ligand}}$) and 1,1′-bi-3,3′-ethynyl-2,2′-binaphthol ($\mathbf{2}_{\text{ligand}}$) [30] are discussed by ECD calculations. We aim to address the structure–property relationship of Λ-type POM derivatives. Our work provides a novel idea to design high-dimensional POM-based NLO materials combining with chirality.

2. Computational methods

2.1. Molecular structures

Compounds **1** and **2** were synthesized, while the crystal structures were not available [30]. The structures of compounds **1** and **2** were constructed based on the structures of 1,1′-bi-6,6′-ethynyl-2,2′-binaphthol [31] and arylimido-substituted Lindqvist-type polyoxomolybdate [32]. Compounds $\mathbf{3}_{30^\circ}$, $\mathbf{3}_{70^\circ}$, and $\mathbf{3}_{100^\circ}$ were generated by removing the ethoxyl groups from compound **1**, and the torsion angles between two naphthyl rings (φ-9-1-1′-9′ in Fig. 1) were restrained to 30°, 70°, and 100°, respectively. On the basis of the optimized structure of compound **1**, the structures of compounds **4**, **5**, and **6** were constructed via replacing the ethoxyl groups on 2-2′-sites of 1,1′-binaphthyl by electron donors dimethylsilane [33], ferrocene [34] and acceptor lactone [35], respectively. Compound **4** was optimized without any symmetrical constraint, and other compounds were optimized under C_2 symmetry. According to the crystal structures of 1,1′-binaphthyl derivatives, compound **4** was of *R* stereochemistry, while other compounds were of *S* stereochemistry.

2.2. The static first hyperpolarizability calculations

Geometry optimizations were carried out using ADF2008.01 program [36]. The local density approximation (LDA) characterized by the Vosko–Willk–Nusair (VWN) parametrization [37] for correlation was used. The generalized-gradient approximation (GGA) was employed by using the Becke [38] and Perdew [39] exchange correlation (XC) functional. The zero-order regular approximation (ZORA) [40] was adopted in all the calculations to account for the scalar relativistic effects. The basis functions were Slater-type sets. Triple-ζ plus polarization (TZP) basis sets were used to describe the valence electrons of all atoms. For transition metal Mo atom, a frozen core composed of 1s to 3spd shells was described by means of single Slater functions. Moreover, the value of the numerical integration parameter used to determine the precision of numerical integrals was 6.0. All the structures were optimized in a model solvent accounted for with the conductor-like screening model (COSMO) [41] implemented as part of the ADF code. To define the cavity surrounding molecules, we used the solvent-excluding-surface method and a fine tesserae. The ionic radii, which actually define the size of the solvent cavity the target molecule remains, were chosen to be 1.26 Å for Mo atom, and 1.52 Å, 1.70 Å, 1.55 Å, and 1.20 Å for O, C, N, and H, respectively. The dielectric constant (ε) was set to be 37.5 for modeling the effects of acetonitrile. The following TDDFT calculations were carried out in acetonitrile solvent. The static first hyperpolarizabilities were calculated by the RESPONSE module and the excited state calculations were carried out under the EXCITATIONS module in ADF. The "gradient-regulated connection potential" (GRAC) [42] corrects the Kohn–Sham potential in the outer "asymptotic" region therefore leads to improved virtual orbitals. Our previous work confirmed the efficiency of GRAC on calculating the excited states of large POM systems [43]. Thus GRAC was used to calculate the static first hyperpolarizabilities and electron transitions of studied compounds.

2.3. ECD calculations

Coulomb-attenuating method (CAM-B3LYP) [44] was developed to overcome the deficiencies of B3LYP in dealing with Rydberg and charge-transfer (CT) excitations. The CAM-B3LYP functional improves the ECD calculations of conjugated systems than traditional density functionals, such as B3LYP [44]. For the past few years, the CAM-B3LYP functional has been applied to study the excited properties of large metal-containing systems [45–48]. The ECD spectra of compounds **1** and **2** and their precursors $\mathbf{1}_{\text{ligand}}$ and $\mathbf{2}_{\text{lignad}}$ were calculated by TDDFT/CAM-B3LYP ($\alpha = 0.19$, $\beta = 0.46$, and $\mu = 0.33$) method [49] from the standpoints that DFT are computational cost agreeable for calculating large POMs and these compounds are expected to be CT-excitation-dominated systems [27]. The effective core potential (ECP) basis set LANL2DZ [50] was used to describe the electrons of all atoms in compounds **1** and **2**, while SVP basis set was used to describe all atoms in $\mathbf{1}_{\text{ligand}}$ and $\mathbf{2}_{\text{lignad}}$. For comparison, the ECD spectra of $\mathbf{1}_{\text{ligand}}$ and $\mathbf{2}_{\text{lignad}}$ were also discussed by B3LYP functional. Solvent effect, which proves to have great influence on molecular ECD spectrum [51], was considered with polarizable continuum model (PCM) [52] in acetonitrile reaction field. The lowest 150 excited states were calculated for simulating the ECD spectrum of compounds **1** and **2**, and 40 excited states for $\mathbf{1}_{\text{ligand}}$ and $\mathbf{2}_{\text{ligand}}$. The ECD calculations were carried out in Gaussian 09 program package [53].

To consolidate the absorption spectrum calculations, the UV–Vis and the ECD spectra of compounds $\mathbf{1}_{\text{ligand}}$, $\mathbf{2}_{\text{ligand}}$, **1**, and **2** were also simulated at the GRAC/TZP level by using ADF2008.01 program [54].

Table 1
The torsion angles φ (°) of optimized compounds.

Compound	$\mathbf{1}_{ligand}$	**1**	$\mathbf{2}_{ligand}$	**2**	**4**	**5**	**6**
φ	99.4	100.4	95.7	95.7	−31.5	32.7	69.2

3. Results and discussion

3.1. Structures and electronic properties

The chirality of 1,1′-binaphthyl derivatives originates from relative twisting of two naphthyl rings away from each other due to intramolecular repulsion between adjacent groups on aryl ring. Simultaneously, the π-conjugated fragment between two naphthyl rings is disturbed. It supposes that the torsion angle φ between two naphthyl rings likely affects the chirality and the NLO properties of studied compounds. The optimized torsion angle φ of compounds **1**, **2**, **4**, **5**, **6**, $\mathbf{1}_{ligand}$, and $\mathbf{2}_{ligand}$ are listed in Table 1. The torsion angles φ of compounds **2** and $\mathbf{2}_{lignad}$ are the same, while the torsion angle φ difference between compounds **1** and $\mathbf{1}_{ligand}$ is 1.0°. Thus the POM clusters slightly affect the torsion angle φ. The torsion angle φ difference between compounds **1** and **2** is 4.7°. In compounds **4**, **5**, and **6**, torsion angles φ (negative for *R* stereochemistry and positive for *S*) are −31.5°, 32.7°, and 69.2°, respectively. These torsion angles are subsequently considered as a benchmark in discussing the NLO response.

The frontier molecular orbital (FMO) energy level diagrams for compounds **1**, **2**, **4**, **5**, and **6** are shown in Fig. 2. The highest occupied molecular orbitals (HOMOs) of studied compounds are delocalized over organic segments. HOMO of compound **6** is localized on ferrocene. The lowest unoccupied molecular orbitals (LUMOs) of all compounds are localized on POM cages. It proposes our studied compounds likely to generate large CT transitions. The HOMO energies of studied compounds increase as the following order: **2** < **4** < **5** < **1** < **6**. Among them, the HOMO energy of compound **2** is lower than that of its isomeric compound **1** by 0.2 eV. It supposes that the site of $-C\equiv CArNPMo_6O_{18}$ fragment on 1,1′-binaphthyl affects HOMO energies of studied compounds. Compared with compound **4**, the HOMO energy of compound **5** is shifted up due to the electron-donating nature of dimethylsilane. The HOMO energy of compound **6** is shifted up by 0.6–0.8 eV in comparison with other compounds. While, the LUMO energies of all compounds are similar. It concludes that the organic substituents on 2,2′-sites of 1,1′-binaphthyl modify the HOMOs of studied compounds.

Table 2
The tensor components ($\beta_{ijk} \times 10^{-30}$ esu), total static first hyperpolarizabilities ($\beta_0 \times 10^{-30}$ esu), and anisotropy u (β_{ijj}/β_{iii}) of studied compounds.

Compound	β_{zxx}	β_{xyz}	β_{zzz}	u	β_0
1	929.7	−60.7	289.8	3.21	731.2
2	−322.9	34.6	−125.0	2.58	269.2
4	−109.1	4.7	−114.1	0.96	278.1
5	370.9	−12.0	265.6	1.40	382.7
6	1245.9	−6.7	1104.0	1.13	1408.9

3.2. The static first hyperpolarizabilities

The static first hyperpolarizabilities of studied compounds are calculated under electric-dipole approximation. The total first hyperpolarizability β_0 is defined by $\beta_0 = \sqrt{\beta_x^2 + \beta_y^2 + \beta_z^2}$. The components β_x, β_y, and β_z are the first hyperpolarizability tensors along the *x*-, *y*-, and *z*-axes, respectively. The vector component β_i is defined by $\beta_i = 3/5 \sum_{j=x,y,z} \beta_{ijj}$. For 1,1′-binaphthyl analogs with C_2 symmetry, there are thirteen nonzero tensor components of first hyperpolarizability. Assuming Kleinman symmetry, there are four independent components that are achiral components β_{zzz}, β_{zxx}, and β_{zyy}, and chiral component β_{xyz} [55]. For nonsymmetrical compound **4**, twenty seven tensor components are all nonzero and ten of them are independent. Further more, the 'in-plane nonlinear anisotropy' value u, which is defined as $u = \beta_{ijj}/\beta_{iii}$ [56], is used to evaluate the 2D-NLO responses of studied compounds. It is known that the larger the value of u is, the stronger the 2D-NLO response is. The total first hyperpolarizabilities (β_0), the representative tensor components (β_{ijk}), and the NLO anisotropies (u) of compounds **1**, **2**, **4**, **5**, and **6** are listed in Table 2. The second-order NLO responses versus torsion angle φ in compounds $\mathbf{3}_{30°}$, $\mathbf{3}_{70°}$, and $\mathbf{3}_{100°}$ are plotted in Fig. 3.

Firstly, the effects of torsion angle φ on the static first hyperpolarizability of studied compounds are investigated. For compounds $\mathbf{3}_{30°}$, $\mathbf{3}_{70°}$, and $\mathbf{3}_{100°}$, the torsion angles φ are restricted at 30°, 70°, and 100°, respectively. Fig. 3 shows that the β_0 values decrease in the order of $\mathbf{3}_{30°} > \mathbf{3}_{70°} > \mathbf{3}_{100°}$. Simultaneously, the anisotropy u and the chiral tensor components β_{xyz} increase with the enlarging torsion angle φ. That is, torsion angles φ influence the second-order NLO responses of studied compounds. As the torsion angle φ affects the conjugation of compound, the smaller φ is favorable

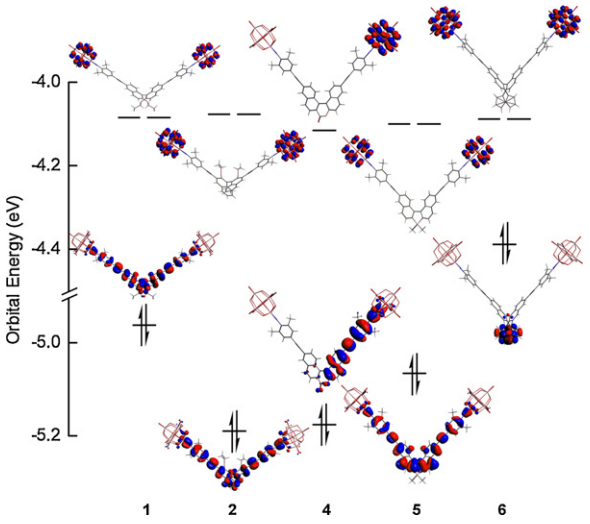

Fig. 2. Frontier molecular orbital energy level diagrams for compounds **1**, **2**, **4**, **5**, and **6**.

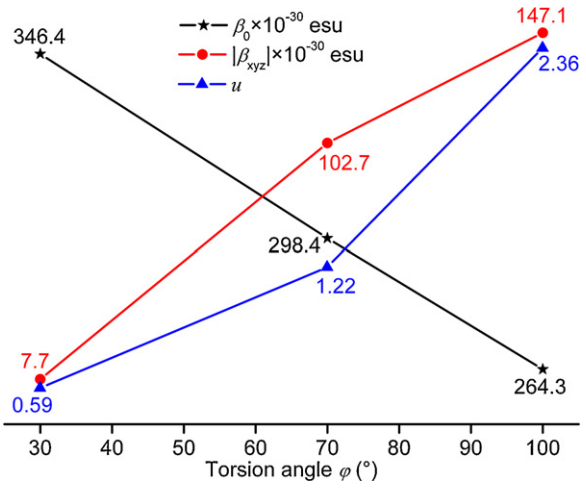

Fig. 3. The second-order NLO responses versus torsion angle φ in compounds $\mathbf{3}_{30°}$, $\mathbf{3}_{70°}$, and $\mathbf{3}_{100°}$.

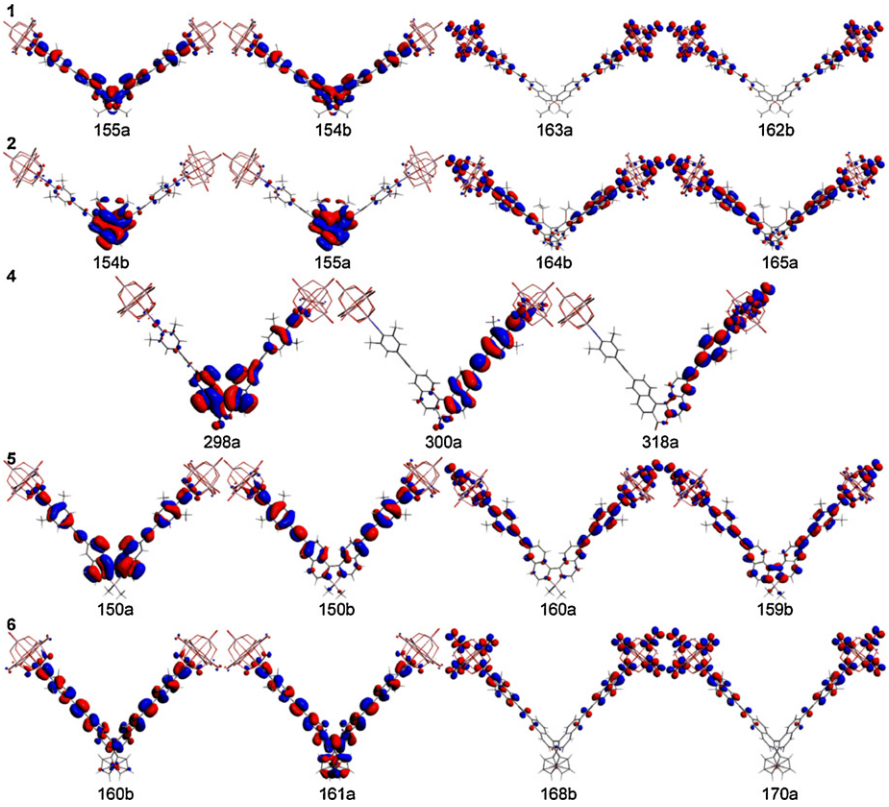

Fig. 4. The dominant molecular orbital transitions of compounds **1**, **2**, **4**, **5**, and **6**.

for enhancing the second-order NLO response. The β_0 value of compound **1** is almost three times as large as that of its isomeric compound **2**, and the anisotropy u of the former is larger than the latter. It is noticed that the torsion angle φ difference between compounds **1** and **2** is of 4.7°, whose contribution to the largely different NLO responses of compounds **1** and **2** is neglectable according to Fig. 3. Hence, the $-C{\equiv}CArNPMo_6O^{18}$ fragment position on 1,1′-binaphthyl is an important factor to modify the first hyperpoarizability of studied compound.

The β_0 values of compounds **4**, **5**, and **6** are 278.1, 382.7, and 1408.9×10^{-30} esu, respectively. For compounds **4**, **5**, and **6**, the substituents on 2,2′-sites of 1,1′-binaphthyl are lactone, dimethylsilane, and ferrocene, respectively. Their torsion angles φ increase as **4** ≈ **5** < **6**. It is obvious that the substituent effect is a key factor in determining the second-order NLO response. The torsion angles φ of compounds **4** and **5** are almost equal. Thus the different second-order NLO responses of compounds **4** and **5** are likely caused by the nature of substituents on 2,2′-sites of 1,1′-binaphthyl instead of the torsion angles φ. It concludes that the electron-donor substituent on 2,2′-sites of 1,1′-binaphthyl is helpful to enhance the β_0 value, thus enhancing the electron-donating strength of 1,1′-binaphthyl is helpful in increasing the NLO response. The static first hyperpolarizability of compound **6** is largely enhanced by the strong electron donor ferrocene. Further more, compounds **1**, **2**, **4**, **5**, and **6** possess significant u values (0.96–3.21), which demonstrates that they are potentially 2D-NLO materials.

To get more insight into the second-order NLO properties of studied compounds, the absorption spectra of them have been calculated by using TDDFT methods. The calculated transition energies (ΔE), oscillator strengths (f), transition symmetry (S), transition dipole moments along x-, y-, and z-axes (μ_i), and dominant molecular orbital (MO) transitions of studied compounds are listed in Table 3. The second-order polarizability caused by CT transition is proportional to the oscillator strength and inversely proportional to the cube of excitation energy. Thus the transition energy is a decisive factor in the β_0 value [57]. It is seen that the excitation energies of crucial transitions decrease in the order of **4** < **5** < **1** < **6**. The red shifts of absorption bands of studied compounds are attributed to different substituents on 1,1′-binaphthyl, and this behavior significantly enhances the β_0 value.

For compounds **1**, **2**, **5**, and **6** with C_2 symmetry, there are a couple of electronic-dipole-allowed excited states composed of electron transitions in symmetry A (along z-axis) and B (along x-axis), respectively. The crucial excited states of compound **4** originate from the electron transitions in symmetry A along x- and z-axes. The molecular orbitals involved in the dominant electron transitions of compounds **1**, **2**, **4**, **5**, and **6** are shown in Fig. 4. For compounds **1**, **5**, and **6**, the CT transition is mainly from the organic segment to polyanions. While the CT transition in compound **2** is from 1,1′-binaphthyl to polyanions. On the basis of CT analysis on compounds **1** and **2**, it suggests that the site of $-C{\equiv}CArNPMo_6O^{18}$ fragment on 1,1′-binaphthyl affects the CT transitions of studied compounds. The CT transition of compound **4** is also from 1,1′-binaphthyl to polyanions, which is similar to compound **2**. So the electron donor or acceptor on the 1,1′-binaphthyl determines the CT transitions of studied compounds. Herein, the polyanion acts as the electron acceptor, and the organic segment acts as the electron donor. The intense and low-lying CT transitions of studied compounds are x-polarized (B symmetry) and z-polarized (A symmetry), respectively. It is known that the z-polarized transition accounts for the diagonal second-order polarizability tensor term, and x-polarized transition contributes to the off-diagonal second-order polarizability tensor term. The low-lying excitation energies associated with the z-polarized transitions decrease according to the order of **2** > **4** > **5** > **1** > **6**, and those associated with the x-polarized transition decrease as the same order. The lower transition energies would enhance the second-order NLO responses, so the β_0 value of compound **6** is the largest among the

Table 3
Symmetry (S), oscillator strengths (f), excitation energies (ΔE, eV), transition dipole moments (μ_i, a.u.), and dominant molecular orbital (MO) transitions of studied compounds.

Compound	S	f	ΔE(eV)	μ_i			Main transition
				x	y	z	
1	A	0.29	2.28			−2.26	155a → 163a (29%); 154b → 162b (16%); 156a → 165a (14%); 154b → 164b (13%)
	B	0.66	2.26	3.46	−0.23		155a → 162b (45%); 154b → 163a (19%)
2	A	0.32	2.51			−2.27	154b → 164b (25%); 155a → 165a (23%); 156a → 165a (14%); 155b → 164b (14%)
	B	0.75	2.46	−3.50	0.30		154b → 165a (46%); 156a → 164b (13%); 153b → 161a (12%); 155b → 165a (10%)
4	A	0.88	2.40	−2.78	0.11	−2.69	300a → 318a (52%); 298a → 318a (12%)
5	A	0.42	2.32			−2.72	150a → 160a (36%); 150b → 159b (32%); 151a → 160a (13%)
	B	0.44	2.30	2.79	−0.12		150b → 160a (43%); 150a → 159b (33%)
6	A	0.23	1.79			−2.28	160b → 168b (62%); 161a → 170a (20%)
	B	0.28	1.77	2.53	−0.13		160b → 170a (67%); 161a → 168b (18%)

studied compounds. The transition dipole moment is mainly along z-axis and x-axis which is responsible for the 2D-NLO responses. In addition, there is a small transition dipole moment on y-axis owing to the twisted nature between two naphthyl rings, which bestows our studied compound a weak NLO response along this axis. This third dimensional NLO response is more prospective in high-dimensional NLO materials.

3.3. Optical active properties

The ultraviolet–visible (UV–Vis) and the ECD spectra of compounds **1**, **2**, $\mathbf{1}_{\text{ligand}}$, and $\mathbf{2}_{\text{ligand}}$ are calculated by TDDFT/CAM-B3LYP method. For comparison, the UV–Vis and ECD spectra of compounds $\mathbf{1}_{\text{ligand}}$ and $\mathbf{2}_{\text{ligand}}$ are also studied by TDDFT/B3LYP. The simulated and the experimental UV–Vis spectra are shown in Fig. 5. The calculated excitation energies, rotatory strengths, and the simulated and the experimental ECD spectra are plotted in Fig. 6.

For compound $\mathbf{1}_{\text{ligand}}$, the absorption bands α ($\Delta E \approx 4.1$ eV) and β ($\Delta E \approx 5.0$ eV) are well reproduced by CAM-B3LYP functional, while B3LYP functional underestimates the absorption energies of these bands by around 0.3 eV. Similarly, both the shapes and absorption peaks of UV–Vis spectra for compound $\mathbf{2}_{\text{ligand}}$ are better described by CAM-B3LYP functional. The UV–Vis spectra of compound $\mathbf{2}_{\text{ligand}}$ are slightly blue-shifted compared with those of compound $\mathbf{1}_{\text{ligand}}$, while the shapes are almost same. The experimental UV–Vis spectra of compounds **1** and **2** show a broad band at $\Delta E \approx 3.1$ eV (band α) and two overlapped broad bands at $\Delta E \approx 4.3$ eV (band β) and $\Delta E \approx 5.5$ eV (band γ). For convenient comparison with the experimental values, the simulated UV–Vis bands of compounds **1** and **2** are blue-shifted by 0.4 eV, as well as for ECD spectra. Compared with $\mathbf{1}_{\text{ligand}}$ and $\mathbf{2}_{\text{ligand}}$, compounds **1** and **2** show additional low-energy absorption band at $\Delta E \approx 3.1$ eV (band α) and the strengthened UV–Vis band at $\Delta E \approx 4.0$ eV (band β).

The optical rotatory absorptions corresponding to each excited states are used to simulate the ECD spectra of compounds **1** and **2** and their precursors $\mathbf{1}_{\text{ligand}}$ and $\mathbf{2}_{\text{ligand}}$. Fig. 6 shows that the ECD spectra of $\mathbf{1}_{\text{ligand}}$ and $\mathbf{2}_{\text{ligand}}$ are well reproduced by CAM-B3LYP/SVP, while the results from B3LYP/SVP calculations are red-shifted. The ECD bands I of compounds $\mathbf{1}_{\text{ligand}}$ and $\mathbf{2}_{\text{ligand}}$ are assigned to the experimental bands α. The pair of Cotton effects in

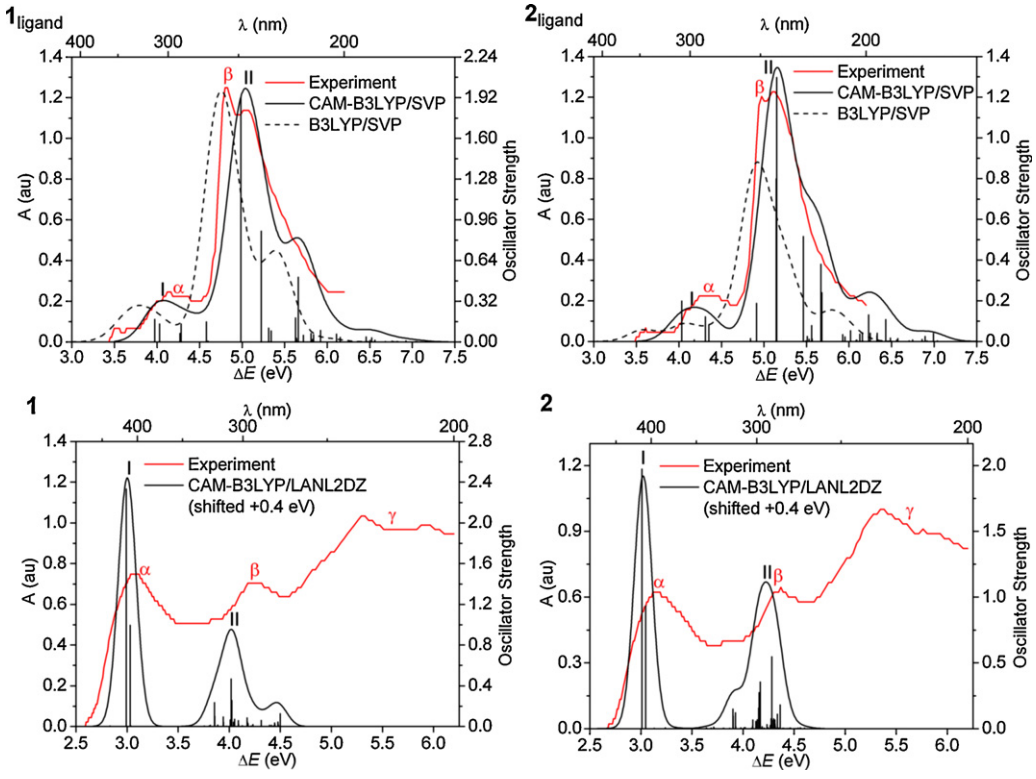

Fig. 5. Simulated UV–Vis spectra together with experimental results are shown, where the experimental data is abstracted from graphical materials in literature [30]. For compounds **1** and **2**, the calculated excitation energies are shifted +0.4 eV. Black bars are oscillator strengths to each excited states obtained by CAM-B3LYP/SVP. The experimental bands are marked by Greek letters (α, β and γ) and the simulated bands at the CAM-B3LYP/SVP level are marked by Roman numerals (I and II).

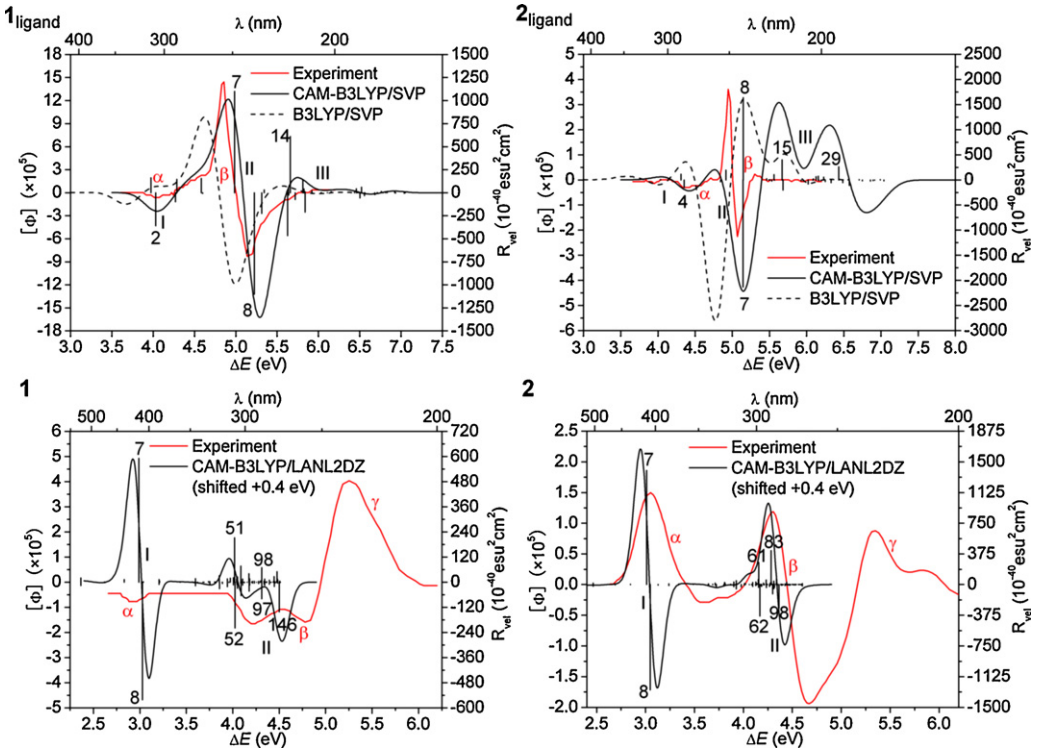

Fig. 6. Simulated ECD spectra together with experimental results are shown, where the experimental data is abstracted from graphical materials in literature [30]. For compounds **1** and **2**, the calculated excitation energies are shifted +0.4 eV. The indication scheme is the same as in Fig. 5. Additionally, the crucial rotatory strengths are marked by digits (correspond to the "Excitation" term in Table S1, Supplementary data).

ECD band II of precursor account for those in the experimental ECD band β. The ECD band III of precursor is not observed in experiment. Compared with $\mathbf{1}_{ligand}$, the ECD spectrum of $\mathbf{2}_{ligand}$ has a compact pair of Cotton effects in the second band, which can be explained by the intimate excited states 7 and 8 of $\mathbf{2}_{ligand}$. In contrast to $\mathbf{1}_{ligand}$ and $\mathbf{2}_{ligand}$, the ECD spectra of compounds **1** and **2** have an additional pair of Cotton effects (band I) corresponding to the UV–Vis absorption bands around 3.1 eV, which are mainly simulated by the excited states 7 and 8. The simulated ECD bands II of compounds **1** and **2** are assigned to the experimental ECD bands β.

To further inspect the ECD spectrum differences between compounds and their precursors, the crucial electron transitions contributing to the ECD bands are studied. The dominant electron transitions, which are responsible for the optical rotatory absorptions, are analyzed by electron density difference maps (EDDMs) of the corresponding excited states (see Supplementary data). EDDM is calculated by GaussSum software package [58]. It shows that the ECD bands I of compounds **1** and **2** are assigned to the CT transitions from π orbitals delocalized over 1,1′-binaphthyl and ethynyl segment to d orbitals of Mo atoms in polyanions. The ECD band II of compound **1** mainly originates from the CT transitions from π orbitals localized on arylimido to d orbitals of Mo atoms in polyanions and the CT transitions from O atoms to Mo atoms in polyanions. While for compound **2**, the CT transitions from π orbitals delocalized over 1,1′-binaphthyl and ethynyl segments to d orbitals of Mo atoms in polyanions are mainly responsible for the optical rotatory absorptions in the ECD band II.

To consolidate the linear optical calculations, the UV–Vis and the ECD spectra of compounds $\mathbf{1}_{ligand}$, $\mathbf{2}_{ligand}$, **1**, and **2** are also simulated at the GRAC/TZP level. The results show that GRAC/TZP method underestimates the excitation energies of our studied compounds by around 0.4 eV for precursors and 1.5 eV for hybrid compounds, while the UV–Vis shapes and the electron transitions for studied compounds are quite similar to the results obtained by using CAM-B3LYP hybrid functional (Supplementary data). Therefore the results obtained by GRAC and CAM-B3LYP consolidate with each other in absorption intensity and the origin of excitation. CAM-B3LYP hybrid functional is superior to GRAC model in reproducing the absorption spectra of our studied compounds for better depicting the excitation energies, which is reasonable in that the coulomb-attenuating method CAM-B3LYP is good at dealing with charge-transfer excitation systems [44].

4. Conclusions

In this paper, we investigate the static first hyperpolarizabilities and the ECD spectra of Λ-type chiral compounds which are composed of Lindqvist-type polyanions linked by 1,1′-binaphthyl through π-bridge arylimido. To get the structure–property relationship of these compounds, the effects of substituents and torsion angles between two naphthyl rings on the second-order NLO response are discussed. The optical activities of these compounds are discussed by ECD spectra, and the electron transition contributions are assigned. The main contributions are as follows: (i) The smaller torsion angle between two naphthyl rings is helpful in enhancing second-order NLO responses of studied compounds as the torsion angle affect the delocalized degree of compound. Comparing with electron acceptor, the introduction of donors significantly enhances the first hyperpolarizabilities of compounds as the electron-donating ability of organic fragment is increased when the electron-donor is attached to the 1,1′-binaphthyl. (ii) The substituents on 2,2′-sites of 1,1′-binaphthyl two-fold control the second-order NLO responses of studied compounds by the nature of electron acceptor or donor and constraining the torsion angle between two naphthyl rings. Therefore, an outstanding NLO compound is obtained when the substituent is ferrocene. (iii) These Λ-type compounds are potentially 2D-NLO materials with compound **1** owing the largest 'in-plane nonlinear anisotropy'. (iv) The

optical activities of compounds **1** and **2** and their respective precursors were discussed by ECD calculations. The simulated ECD spectra are reliable for having an excellent comparison with the experimental CD spectra. For the bonding of POM clusters to 1,1′-binaphthyl-based precursors, additional ECD bands are observed and assigned to the CT transitions from 1,1′-binaphthyl and π-bridge fragments to POM cages. Some different electron transition origins for the counterpart ECD bands of compound **1** and **2** are found, which are responsible for their different ECD spectra observed in experiment.

Our work highlights a novel multifunctional organic-POM hybrid bearing high-dimensional NLO property and chirality. The studied compounds are promising in NLO material researches due to their controllable chiralities, electron transition properties, and second-order NLO responses. This work provides theoretical evidence to design POM-based chiral Λ-type NLO materials, and it should be useful to guide the experimental design in this area.

Acknowledgements

The authors thank the computational support from Research Center of Agriculture and Medicine Gene Engineering of Ministry of Education of Northeast Normal University. The financial support from NSFC (20971020 and 21073030), the Science and Technology Development Planning of Jilin Province (20100104), and Doctoral Fund of Ministry of Education of China (20100043120007) is gratefully acknowledged. The computational support from Dr. Yu-He Kan is appreciated.

Appendix A. Supplementary data

Supplementary data associated with this article can be found, in the online version, at doi:10.1016/j.jmgm.2011.09.005.

References

[1] A. Dolbecq, E. Dumas, C.R. Mayer, P. Mialane, Hybrid organic–inorganic polyoxometalate compounds: from structural diversity to applications, Chem. Rev. 110 (2010) 6009–6048.
[2] N. Dupré, P. Rémy, K. Micoine, C. Boglio, S. Thorimbert, E. Lacôte, B. Hasenknopf, M. Malacria, Chemoselective catalysis with organosoluble Lewis acidic polyoxotungstates, Chem. Eur. J. 16 (2010) 7256–7264.
[3] K. Micoine, B. Hasenknopf, S. Thorimbert, E. Lacôte, M. Malacria, Chiral recognition of hybrid metal oxide by peptides, Angew. Chem. Int. Ed. 48 (2009) 3466–3468.
[4] V. Soghomonian, Q. Chen, R.C. Haushalter, J. Zubieta, C.J. O'Connor, An inorganic double helix: hydrothermal synthesis, structure, and magnetism of chiral $[(CH_3)_2NH_2]K_4[V_{10}O_{10}(H_2O)_2(OH)_4(PO_4)_7]\cdot 4H_2O$, Science 259 (1993) 1596–1599.
[5] H.Y. An, E.B. Wang, D.R. Xiao, Y.G. Li, Z.M. Su, L. Xu, Chiral 3D architectures with helical channels constructed from polyoxometalate clusters and copper–amino acid complexes, Angew. Chem. Int. Ed. 45 (2006) 904–908.
[6] F. Xiao, J. Hao, J. Zhang, C. Lv, P. Yin, L. Wang, Y. Wei, Polyoxometalatocyclophanes: controlled assembly of polyoxometalate-based chiral metallamacrocycles from achiral building blocks, J. Am. Chem. Soc. 132 (2010) 5956–5957.
[7] Y. Hou, X. Fang, C.L. Hill, Breaking symmetry: spontaneous resolution of a polyoxometalate, Chem. Eur. J. 13 (2007) 9442–9447.
[8] J. Zhang, J. Hao, Y. Wei, F. Xiao, P. Yin, L. Wang, Nanoscale chiral rod-like molecular triads assembled from achiral polyoxometalates, J. Am. Chem. Soc. 132 (2010) 14–15.
[9] L.K. Yan, X. López, J.J. Carbó, R. Sniatynsky, D.C. Duncan, J.M. Poblet, On the origin of alternating bond distortions and the emergence of chirality in polyoxometalate anions, J. Am. Chem. Soc. 130 (2008) 8223–8233.
[10] T. Verbiest, S.V. Elshocht, M. Kauranen, L. Hellemans, J. Snauwaert, C. Nuckolls, T.J. Katz, A. Persoons, Strong enhancement of nonlinear optical properties through supramolecular chirality, Science 282 (1998) 913–915.
[11] F. Hache, Quantum calculation of the second-order hyperpolarizability of chiral molecules in the "one-electron" model, J. Phys. Chem. A 114 (2010) 10277–10286.
[12] P. Fischer, F. Hache, Nonlinear optical spectroscopy of chiral molecules, Chirality 17 (2005) 421–437.
[13] G. Matar, J. Duboisset, E. Benichou, G. Bachelier, I. Russier-Antoine, C. Jonin, D. Ficheux, P.F. Brevet, F. Besson, Second harmonic generation, a new approach for analyzing the interfacial properties of a short tryptophan-rich peptide, Chem. Phys. Lett. 500 (2010) 161–166.
[14] V. Nucciotti, C. Stringari, L. Sacconi, F. Vanzi, L. Fusi, M. Linari, G. Piazzesi, V. Lombardi, F.S. Pavone, Probing myosin structural conformation in vivo by second-harmonic generation microscopy, Proc. Nat. Acad. Sci. U. S. A. 107 (2010) 7763–7768.
[15] R.D. Wampler, D.J. Kissick, C.J. Dehen, E.J. Gualtieri, J.L. Grey, H.-F. Wang, D.H. Thompson, J.-X. Cheng, G.J. Simpson, Selective detection of protein crystals by second harmonic microscopy, J. Am. Chem. Soc. 130 (2008) 14076–14077.
[16] J.Y. Niu, X.Z. You, C.Y. Duan, H.K. Fun, Z.Y. Zhou, A novel optical complex between an organic substrate and a polyoxometalate. Crystal and molecular structure of α-$H_4SiW_{12}O_{40}\cdot 4HMPA\cdot 2H_2O$ (HMPA = hexamethylphosphoramide), Inorg. Chem. 35 (1996) 4211–4217.
[17] L.G.S. Brooker, R.H. Sprague, Color and constitution IV. The absorption of phenol blue, J. Am. Chem. Soc. 63 (1941) 3214–3215.
[18] C. Yao, L.K. Yan, W. Guan, C.G. Liu, P. Song, Z.M. Su, Prediction of second-order optical nonlinearity of porphyrin–metal–polyoxometalate sandwich compounds, Dalton Trans. 39 (2010) 7645–7649.
[19] M. Janjua, W. Guan, L. Yan, Z.M. Su, M. Ali, I.H. Bukhari, Prediction of robustly large molecular second-order nonlinear optical properties of terpyridine-substituted hexamolybdates: structural modelling towards a rational entry to NLO materials, J. Mol. Graphics Modell. 28 (2010) 735–745.
[20] M. Janjua, W. Guan, L.K. Yan, Z.M. Su, A. Karim, J. Akbar, Quantum chemical design for enhanced second-order NLO response of terpyridine-substituted hexamolybdates, Eur. J. Inorg. Chem. (2010) 3466–3472.
[21] J.-D. Compain, P. Mialane, A. Dolbecq, J. Marrot, A. Proust, K. Nakatani, P. Yu, F. Sécheresse, Second-order nonlinear optical properties of polyoxometalate salts of a chiral stilbazolium derivative, Inorg. Chem. 48 (2009) 6222–6228.
[22] Y.M. Xie, Q.S. Zhang, Z.G. Zhao, X.Y. Wu, S.C. Chen, C.Z. Lu, New optical supramolecular compound constructed from a polyoxometalate cluster and an organic substrate, Inorg. Chem. 47 (2008) 8086–8090.
[23] L. Xu, E.B. Wang, Z. Li, D.G. Kurth, X.G. Du, H.Y. Zhang, C. Qin, Preparation and nonlinear optical properties of ultrathin composite films containing both a polyoxometalate anion and a binuclear phthalocyanine, New J. Chem. 26 (2002) 782–786.
[24] W. Guan, G.C. Yang, L.K. Yan, Z.M. Su, Prediction of second-order optical nonlinearity of trisorganotin-substituted beta-Keggin polyoxotungstate, Inorg. Chem. 45 (2006) 7864–7868.
[25] L.K. Yan, M.S. Jin, J. Zhuang, C.G. Liu, Z.M. Su, C.C. Sun, Theoretical study on the considerable second-order nonlinear optical properties of naphthylimido-substituted hexamolybdates, J. Phys. Chem. A 112 (2008) 9919–9923.
[26] C. Yao, L.K. Yan, W. Guan, C.G. Liu, P. Song, Z.M. Su, Length-dependent direction-tunable charge-transfer behavior of second-order optical nonlinearity in Keggin-type organosilicone ferivative $[PW_{11}O_{39}(RSi)_2O]^{3-}$: a TDDFT study, J. Cluster Sci. 21 (2010) 69–80.
[27] P. Song, L.K. Yan, W. Guan, C.G. Liu, C. Yao, Z.M. Su, A theoretical study on the efficient reversible redox-based switching of the second-order polarizabilities of two-dimensional nonlinear optical-active donor–acceptor phenanthroline-hexamolybdate, J. Mol. Graphics Modell. 29 (2010) 13–20.
[28] N. Ji, V. Ostroverkhov, M. Belkin, Y.-J. Shiu, Y.-R. Shen, Toward chiral sum-frequency spectroscopy, J. Am. Chem. Soc. 128 (2006) 8845–8848.
[29] K.M. Wiggins, T.W. Hudnall, Q.L. Shen, M.J. Kryger, J.S. Moore, C.W. Bielawski, Mechanical reconfiguration of stereoisomers, J. Am. Chem. Soc. 132 (2010) 3256–3257.
[30] M. Lu, J. Kang, D. Wang, Z. Peng, Enantiopure 1,1′-binaphthyl-based polyoxometalate-containing molecular hybrids, Inorg. Chem. 44 (2005) 7711–7713.
[31] K. Onitsuka, Y. Harada, F. Takei, S. Takahashi, Synthesis of transition metal-poly(yne) polymer possessing chiral acetylene bridges, Chem. Commun. (1998) 643–644.
[32] L.K. Yan, G.C. Yang, W. Guan, Z.M. Su, R.S. Wang, Density functional theory study on the first hyperpolarizabilities of organoimido derivatives of hexamolybdates, J. Phys. Chem. B 109 (2005) 22332–22336.
[33] S. Yasuike, T. Iida, S. Okajima, K. Yamaguchi, H. Seki, J. Kurita, Synthesis and fluxional behavior of dinaphtho[2,1-b;1′,2′-d]-siloles and -germoles, involving the first example of optically active group 14 dinaphthoheterols, Tetrahedron 57 (2001) 10047–10053.
[34] B.M. Foxman, M. Rosenblum, V. Sokolov, N. Khrushchova, Synthesis and structure of 2,2′-binaphthalenediyl-substituted ferrocenes and derived oligomers, Organometallics 12 (1993) 4805–4809.
[35] G. Bringmann, B. Schöner, O. Schupp, K. Peters, E.-M. Peters, H.G. von Schnering, Novel concepts in directed biaryl synthesis, XXXIV. Synthesis, optical resolution, and helimerization of dinaphtho[2,1-b:1′,2′-d]-pyran-4-one, Liebigs Ann. Chem. 1994 (1994) 91–97.
[36] ADF2008.01, SCM, Theoretical Chemistry, Vrije Universiteit, Amsterdam, The Netherlands. Available at: http://www.scm.com, 2008.
[37] S.H. Vosko, L. Wilk, M. Nusair, Accurate spin-dependent electron liquid correlation energies for local spin density calculations: a critical analysis, Can. J. Chem. 58 (1980) 1200–1211.
[38] A.D. Becke, Density-functional exchange-energy approximation with correct asymptotic behavior, Phys. Rev. A 38 (1988) 3098–3100.
[39] J.P. Perdew, Density-functional approximation for the correlation energy of the inhomogeneous electron gas, Phys. Rev. B 33 (1986) 8822–8824.
[40] E. van Lenthe, E.J. Baerends, J.G. Snijders, Relativistic regular two-component Hamiltonians, J. Chem. Phys. 99 (1993) 4597–4610.

[41] C.C. Pye, T. Ziegler, An implementation of the conductor-like screening model of solvation within the Amsterdam density functional package, Theor. Chem. Acc. 101 (1999) 396–408.
[42] M. Gruning, O.V. Gritsenko, S.J.A. van Gisbergen, E.J. Baerends, Shape corrections to exchange-correlation potentials by gradient-regulated seamless connection of model potentials for inner and outer region, J. Chem. Phys. 114 (2001) 652–660.
[43] G.C. Yang, W. Guan, L.K. Yan, Z.M. Su, L. Xu, E.B. Wang, Theoretical study on the electronic spectrum and the origin of remarkably large third-order nonlinear optical properties of organoimide derivatives of hexamolybdates, J. Phys. Chem. B 110 (2006) 23092–23098.
[44] T. Yanai, D.P. Tew, N.C. Handy, A new hybrid exchange-correlation functional using the Coulomb-attenuating method (CAM-B3LYP), Chem. Phys. Lett. 393 (2004) 51–57.
[45] N. Govind, M. Valiev, L. Jensen, K. Kowalski, Excitation energies of zinc porphyrin in aqueous solution using long-range corrected time-dependent density functional theory, J. Phys. Chem. A 113 (2009) 6041–6043.
[46] J. Guthmuller, L. Gonzalez, Simulation of the resonance Raman intensities of a ruthenium–palladium photocatalyst by time dependent density functional theory, Phys. Chem. Chem. Phys. 12 (2010) 14812–14821.
[47] R. Kobayashi, R.D. Amos, The application of CAM-B3LYP to the charge-transfer band problem of the zincbacteriochlorin–bacteriochlorin complex, Chem. Phys. Lett. 420 (2006) 106–109.
[48] B.X. Tian, E.S.E. Eriksson, L.A. Eriksson, Can range-separated and hybrid DFT functionals predict low-lying excitations? A Tookad case study, J. Chem. Theory Comput. 6 (2010) 2086–2094.
[49] O. Julinek, V. Setnicka, N. Miklasova, M. Putala, K. Ruud, M. Urbanova, Determination of molecular structure of bisphenylene homologues of BINOL-based phosphoramidites by chiroptical methods, J. Phys. Chem. A 113 (2009) 10717–10725.
[50] P.J. Hay, W.R. Wadt, Ab initio effective core potentials for molecular calculations. Potentials for the transition metal atoms Sc to Hg, J. Chem. Phys. 82 (1985) 270–283.
[51] J. Kongsted, T.B. Pedersen, A. Osted, A.E. Hansen, K.V. Mikkelsen, O. Christiansen, Solvent effects on rotatory strength tensors 1. Theory and application of the combined coupled cluster/dielectric continuum model, J. Phys. Chem. A 108 (2004) 3632–3641.
[52] J. Tomasi, B. Mennucci, R. Cammi, Quantum mechanical continuum solvation models, Chem. Rev. 105 (2005) 2999–3094.
[53] M.J. Frisch, G.W. Trucks, H.B. Schlegel, G.E. Scuseria, M.A. Robb, J.R. Cheeseman, G. Scalmani, V. Barone, B. Mennucci, G.A. Petersson, H. Nakatsuji, M. Caricato, X. Li, H.P. Hratchian, A.F. Izmaylov, J. Bloino, G. Zheng, J.L. Sonnenberg, M. Hada, M. Ehara, K. Toyota, R. Fukuda, J. Hasegawa, M. Ishida, T. Nakajima, Y. Honda, O. Kitao, H. Nakai, T. Vreven, J.A. Montegomery Jr., J.E. Peralta, F. Ogliaro, M. Bearpark, J.J. Heyd, E. Brothers, K.N. Kudin, V.N. Staroverov, R. Kobayashi, J. ormand, K. Raghavachari, A. Rendell, J.C. Burant, S.S. Iyengar, J. Tomasi, M. Cossi, N. Rega, J.M. Millam, M. Klene, J.E. Knox, J.B. Cross, V. Bakken, C. Adamo, J. Jaramillo, R. Gomperts, R.E. Stratmann, O. Yazyev, A.J. Austin, R. Cammi, C. Pomelli, J.W. Ochterski, R.L. Martin, K. Morokuma, V.G. Zakrzewski, G.A. Voth, P. Salvador, J.J. Dannenberg, S. Dapprich, A.D. Daniels, O. Farkas, J.B. Foresman, J.V. Ortiz, J. Cioslowski, D.J. Fox, Gaussian 09, Revision A. 01, Gaussian, Inc., Wallingford CT, 2009.
[54] J. Autschbach, T. Ziegler, S.J.A. van Gisbergen, E.J. Baerends, Chiroptical properties from time-dependent density functional theory. I. Circular dichroism spectra of organic molecules, J. Chem. Phys. 116 (2002) 6930–6940.
[55] J.D. Byers, J.M. Hicks, Electronic spectral effects on chiral surface second harmonic generation, Chem. Phys. Lett. 231 (1994) 216–224.
[56] S. Di Bella, I. Fragala, Two-dimensional characteristics of the second-order nonlinear optical response in dipolar donor–acceptor coordination complexes, New J. Chem. 26 (2002) 285–290.
[57] D.R. Kanis, M.A. Ratner, T.J. Marks, Calculation and electronic description of quadratic hyperpolarizabilities. Toward a molecular understanding of NLO responses in organotransition metal chromophores, J. Am. Chem. Soc. 114 (1992) 10338–10357.
[58] N.M. O'Boyle, A.L. Tenderholt, K.M. Langner, cclib: a library for package-independent computational chemistry algorithms, J. Comp. Chem. 29 (2008) 839–845.